AIP | Review of Scientific Instruments

High-throughput on-the-fly scanning ultraviolet-visible dual-sphere spectrometer

Slobodan Mitrovic, Earl W. Cornell, Martin R. Marcin, Ryan J. R. Jones, Paul F. Newhouse, Santosh K. Suram, Jian Jin, and John M. Gregoire

Citation: Review of Scientific Instruments **86**, 013904 (2015); doi: 10.1063/1.4905365
View online: http://dx.doi.org/10.1063/1.4905365
View Table of Contents: http://scitation.aip.org/content/aip/journal/rsi/86/1?ver=pdfcov
Published by the AIP Publishing

High-throughput on-the-fly scanning ultraviolet-visible dual-sphere spectrometer

Slobodan Mitrovic,[1,a)] Earl W. Cornell,[2] Martin R. Marcin,[1] Ryan J. R. Jones,[1] Paul F. Newhouse,[1] Santosh K. Suram,[1] Jian Jin,[2] and John M. Gregoire[1,a)]
[1]*Joint Center for Artificial Photosynthesis, California Institute of Technology, Pasadena, California 91125, USA*
[2]*Engineering Division, Lawrence Berkeley National Laboratory, Berkeley, California 94720, USA*

(Received 10 October 2014; accepted 21 December 2014; published online 13 January 2015)

We have developed an on-the-fly scanning spectrometer operating in the UV-visible and near-infrared that can simultaneously perform transmission and total reflectance measurements at the rate better than 1 sample per second. High throughput optical characterization is important for screening functional materials for a variety of new applications. We demonstrate the utility of the instrument for screening new light absorber materials by measuring the spectral absorbance, which is subsequently used for deriving band gap information through Tauc plot analysis. © *2015 AIP Publishing LLC.* [http://dx.doi.org/10.1063/1.4905365]

I. INTRODUCTION

Many next generation technologies rely upon the development of solid state materials whose material function involves specific interactions with solar radiation. For photovoltaic and photoelectrochemical technologies, the primary functional material is a light absorber which exhibits high absorption at wavelengths below that of the band gap. Other important components such as anti-reflection coatings and transparent conducting oxides require high transmittance. Substantial materials research and development efforts for these applications are underway with combinatorial materials science efforts playing an important role in the discovery of new materials.[1]

Optical characterization, particularly in the visible and near-infrared (NIR) regions, is important for evaluating material performance for these and other applications. In combinatorial experiments, the maximum requisite characterization throughput is that of the material synthesis technique. Recent advances in high throughput synthesis, in particular, fabrication of composition libraries via high speed inkjet printing, have expanded the synthesis throughput to above 10^5 samples per day per instrument.[2,3] Developing optical characterization methods that can match this throughput requires new concepts for optical characterization instruments. We describe here an on-the-fly spectrometry instrument that satisfies this throughput requirement and acquires both transmission and reflections spectra from stationary plates by continuously moving dual integrating spheres.

Combinatorial optical characterization experiments have been developed to measure optical signals for specific applications, though the experiments were not necessarily engineered for high throughput operation. Such measurements include the photoluminescence of phosphors,[4] the spectral reflectance to quantify the color of decorative films,[5] and the thin film optical interference pattern to measure film thickness and etch rate.[6] Fluorescence screening of combinatorial libraries, in particular, has reached high-throughput levels.[7,8]

For solar energy applications, several studies have mapped optical properties of composition libraries to identify transparent conductive oxides,[9–11] with the most comprehensive technique described by Perkins *et al.* using a combination of a FTIR spectrometer and a fiber optic instrument.[9] The configuration of the latter instrument included an optical fiber with a lens to focus incident light on the sample and two additional fibers to collect both transmitted and reflected lights. While the detailed geometry of the fibers is not discussed, given the limited solid angle of detection with respect to the planar sample, the measurements likely included the direct transmission and specular reflection.

In the present instrument, two integrating spheres are placed normal to the sample plate and collect a large solid angle for both transmitted and reflected lights, providing the ability to capture diffuse scattered intensity, enabling characterization of rough films or particulate samples. This design aspect of the instrument is particularly important for combinatorial materials science applications where the morphology of the film may change as a function of composition and the optical experiment cannot be tailored to each sample.

By employing transparent substrates and measuring both transmittance and total reflection, the instrument can quantitatively and accurately describe the spectral absorbance of each sample. By coupling the integrating spheres with a bright illumination source and synchronizing the data acquisition with continuous translation of the spheres, ultra-high throughput optical characterization is performed. The technique is applied to the high throughput mapping of the optical band gap in a pseudo-quaternary metal oxide composition library, prepared by unfolding the 4-component composition space as a grid of discrete samples and depositing each mixture of metal precursors by inkjet printing.[12] The results demonstrate the high data quality obtained during on-the-fly data acquisition, which enables sample throughput of

a)Authors to whom correspondence should be addressed. Electronic addresses: mitrovic@caltech.edu and gregoire@caltech.edu

10^4-10^5 samples per day, comparable to that of state-of-the-art high throughput synthesis.

II. SCANNING UV-VISIBLE (UV-VIS) SPECTROMETER

A. The apparatus

All the basic components of the instrument are shown in Fig. 1. The light source is a 200 W Hg(Xe) arc lamp (Oriel Apex, Newport Corporation) with a rear side reflector and a collimating lens which directs a 33 mm diameter beam through an electronically controllable shutter unit and then into the focusing lens assembly that efficiently illuminates the optical fiber. Both components are supplied by Newport. This assembly provides illumination over a spectral range from UV to NIR. A solarization resistant optical fiber (model XSR fiber by Ocean Optics, Inc.), 115 μm in diameter, is connected to the fiber illumination assembly via SMA 905 connection and delivers the light to the illumination port on the top of the upper integrating sphere (Model ISP-50-8-R-GT, Ocean Optics, Inc., with a 50 mm diameter PTFE-coated sphere and an 8 mm diameter opening). The illumination port is fitted with a focusing lens that was adjusted so that it produces an approximately 1 mm spot in the sample plane under the integrating sphere, at an incident angle of 8°. The light is collected from this upper, labeled #8 in Fig. 1, and also the lower integrating sphere (Model AT-IS-1, Spectral Products, Inc., with 25 mm diameter spectralon®-coated sphere, #9 in Fig. 1).

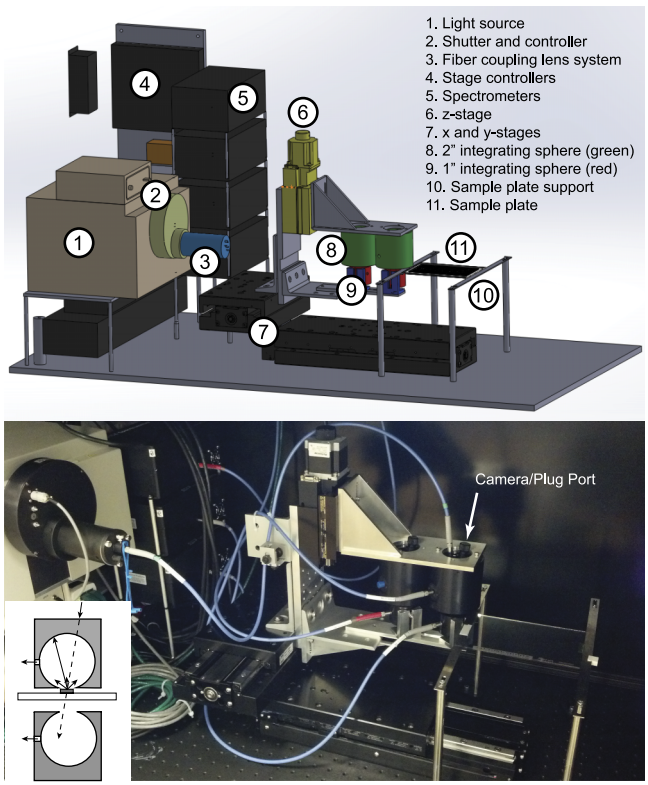

FIG. 1. (Top) The schematic of the essential elements of the UV-Vis apparatus and (Bottom) the photograph of the UV-Vis instrument. The inset shows the principle of the simultaneous measurement of total reflectance and transmittance in the dual integrating sphere setup.

The light gathered by each of the integrating spheres is transmitted through a separate 300 μm diameter solarization resistant patch cord (Model QR300-1-SR, Ocean Optics, Inc.) into a dedicated, separate transmission and reflection spectrometers (both model SM303, Spectral Products, Inc.). These spectrometers are equipped with a thermoelectrically cooled thin back-illuminated silicon CCD with 1024 elements and a large 200 μm slit for highest light throughput, at the expense of wavelength resolution. While the wavelength pixel resolution is only about 1 nm/pixel (1000 nm range of the spectrometer divided by 1024 pixels), the overall resolution is about 7 nm, limited by the slit which is imaged over about 11 pixels of the CCD (taking into account the spectrometer magnification factor of 1.33; 200 μm multiplied by 1.33 and divided by 24 μm size pixel). The resolution calculation assumes that one pixel on each side of the slit image is needed for resolving spectral lines (1 pixel to the left + 11 pixels of the imaged slit + 1 pixel to the right, all multiplied by the wavelength pixel resolution and divided by two for full width at half maximum).

The useful spectral range of the apparatus is 350-1000 nm, limited by the light source on the low wavelength end and by the fiber optic cables on the high end. The XSR patch cords have the highest transmission from 180-800 nm, integrating sphere coatings 200-2500 nm, Hg(Xe) lamp 350-2500 nm, and SM303 about 150-1150 spread with good quantum efficiency from 200-1050 nm. Demonstration of the usable part of the spectrum is presented in Fig. 2(a).

The two integrating spheres are mounted rigidly with respect to each other. A set of two linear stages (FM series, Dover Motion Systems) move the integrating sphere assembly in the x-y plane with a range greater than 150 by 100 mm. The z-stage is capable of lifting the upper integrating sphere and is typically not used during scanning. The stages and the shutter are controlled by a single motion controller unit (DMC 4143, Galil Motion Control, Inc.), which is connected to a computer unit over Ethernet.

The apparatus can also operate in the NIR. A second set of integrating spheres for the NIR light path is mounted next to the UV-Vis integrating spheres (another pair of integrating spheres next to #8 and #9 in Fig. 1). When both UV-Vis and NIR operations are combined, a bifurcated Y patch cord is used to take the light from the arc lamp via separate UV-Vis and Vis-NIR fiber cords into the respective upper integrating spheres. The outputs from the NIR dedicated integrating spheres are taken to InGaAs based, thermoelectrically cooled 512 rectangular pixel (25 × 250 μm) spectrometers (SM304-512-2.5, Spectral Products, Inc.), with wavelength range of 900-2500 nm and 23 nm spectral resolution.

The measurements performed by the UV-Vis scanner apparatus are transmittance and total reflectance. Therefore, we use this technique with samples on transparent substrates. Typically, our experiments investigate approximately 1800 one square millimeter samples deposited on a 101 mm × 152 mm × 2.2 mm borosilicate glass plate (Hartford Glass, Inc.), which is coated with a 400 nm electrically conductive layer of fluorinated tin oxide (FTO,TEC15 coating, Corning, Inc.). The glass plate is suspended between two 1.6 mm (1/16 inch) thick stainless steel bars and supported by 0.127 mm

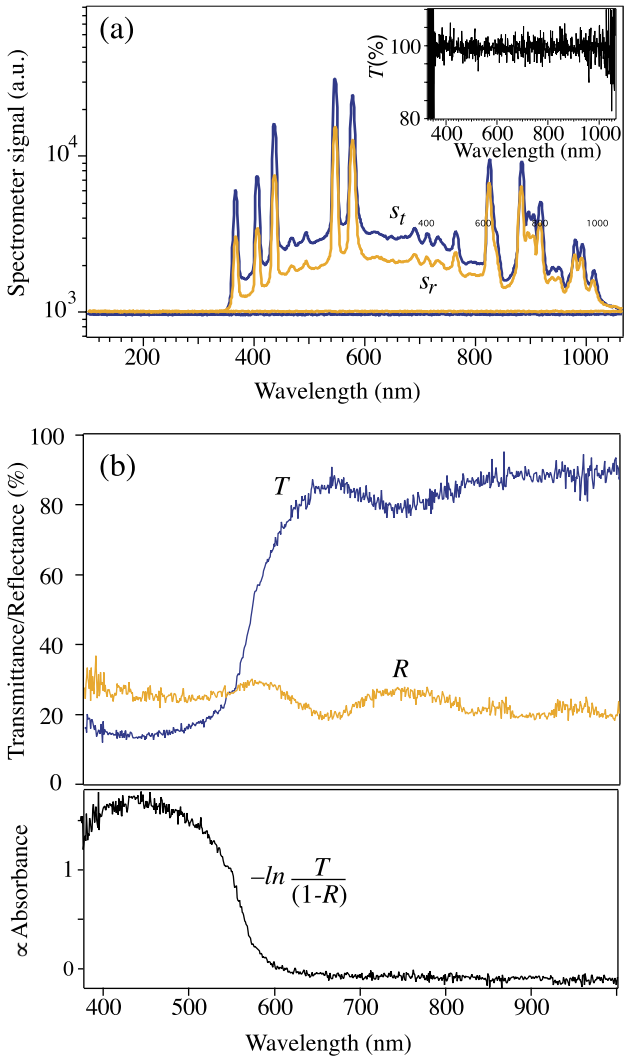

FIG. 2. Examples of collected spectra from Fe_2O_3 thin films. All plots are the result of a single 7 ms scan. (a) Signals from the light collected in transmission s_r and reflection s_t from the sample and the electronic noise levels of the corresponding spectrometers. The inset shows the usable range of wavelengths by showing the calculated transmittance through transparent substrate, with no sample, as used for reference acquisition. (b) Spectra for transmittance and reflectance through the thin film sample, and the value calculated from these two that is proportional to the absorbance of the sample.

(36 gauge) stainless steel tabs on both sides of the plate that are spot welded onto the bars. The left bar features three dowel pins which define the position of the plate with respect to the instrument. The coordinate system of dowel pins is essential for the automated alignment. We discuss this further in Subsection II B. The right bar also holds a diffuse reflectance standard (Spectralon® standard, model CSTM-12, LabSphere, Inc.), with 98%-99% reflectance from 250 to 2000 nm.

During operation, the upper integrating sphere is at most a few hundred micrometers above the substrate, while the lower integrating sphere is about 6-10 mm below. The distance of the lower integrating sphere accommodates the 7.9 mm thick reflectance standard but also ensures that a negligible amount of light is returned from the opening of the lower sphere into the upper sphere.

Finally, the upper integrating sphere must have a reflective plug in the second top-side port in order to collect total reflectance signal. However, during the optimization and alignment of the instrument, the plug can be replaced by an Ethernet camera with a pinhole lens to align the light source to the array of samples.

B. Automation control and data acquisition

A custom automation software application was built in Microsoft Visual Studio using C# and runs under Microsoft Windows. The software interfaces the spectrometers, the motion controller, and the alignment camera to each other. The camera also interfaces via software with the stages to allow the user to align the instrument by looking at the samples under source illumination or position a particular sample for data acquisition.

A material library must be aligned to the optical measurement system and motor axes. During sample loading and alignment, data are not being collected and thus efficient, automated alignment is essential to optimize the throughput of the instrument. Our deposition techniques produce regular grids of samples, but there is typically an offset and a skew with respect to the substrate plate (see top left of Fig. 4).

The offset and the skew are calculated by a separate metrology algorithm using photo-scanned images of the sample plate placed in the coordinate system of three dowel pins (white arrows in Fig. 4 indicate the pins). Upon loading a library plate in the scanning spectrometer, these alignment parameters are refined by an automated procedure. Transmission scans are performed along two rows and two columns of samples around the sample plate perimeter, creating line scans of the integrated transmission over the spectral range. The transmission is lower when scanning over the samples, and identification of transients in the line scans provides sample positions used to precisely align the full grid of samples. This alignment feature is fully automated, requiring no intervention from the operator. It is completed within approximately 3 min and automatically followed by data acquisition.

Since the direction of sample rows does not necessarily coincide with the motion of the x-stage, the continuous scanning is achieved by setting the appropriate linear combination of velocities on the x and y stages. Using the transmission line scan and considering the convolution of the sample spot with the light spots, the illuminated footprint remains within the perimeter of a given sample over a window of approximately 0.2 mm with respect to the center of the sample.

The UV-Vis spectrometer SM303 is capable of acquiring high quality data at the shortest integration time of 7 ms in both transmission and reflection, with the peak signal level at approximately 30%-40% of the saturation level. Therefore, we are able to operate the instrument on-the-fly by collecting data during continual translation of the integrating spheres over the samples, row by row. To ensure that data storage does not interfere with synchronization of the spectrometers and motors, the instrument stores the spectroscopic data into the random access memory of the computer until it reaches the end of a sample row. Then, the entire data set from one row is analyzed by averaging out several spectroscopic

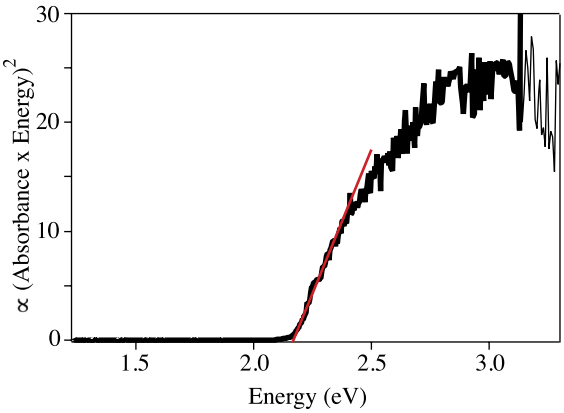

FIG. 3. Tauc plot for the direct allowed bandgap extrapolation. The red line marks the first linear segment which is used to determine the value of the bandgap located at the intercept with the baseline.

measurements over the center of each sample. At the stage velocity of 2 mm/s, we can read typically 4-6 spectra while the light spot is within the 0.2 mm window noted above.

Reference measurements are taken before and after measuring the sample plate. For transmission measurements, an entire row is scanned under the bottom-most and above the top-most row of samples. This is done twice with the lamp on for lamp spectrum reference t, accounting for the absorption of the substrate, and once with the lamp off for the dark spectrum reference (d_t), which comes from the noise in the spectrometer. For reflectance measurements, we acquire both the reference spectrum r and the dark reference d_r over the diffuse reflectance standard, before and after row-by-row scanning. Fig. 2(a) shows examples of these four measurements. The noise level for both spectrometers is similar, but the absolute values are noticeably different. The inset shows the full spectrometer range of the transmittance for the reference, i.e., the glass plate, with the maximum root mean square noise of about 2%-5% in the spectral range of 375-1000 nm. Averaging over multiple 7 ms scans lowers the noise level considerably. The noise level is comparable in both UV-Vis spectrometers.

The entire process of data acquisition is automatic. Other modes of scanning are also available within the software, which include single point acquisitions, scans of selections of a subset of samples, using either on-the-fly or point-by-point data acquisition. A sample plate with over 1800 individual samples can be scanned in under 30 min, giving us a scan rate better than 1 Hz.

C. Data processing

The dark and reference spectra are used to calculate the fractional spectral transmission (T) and reflection (R) from the lower and upper integrating sphere signals, s_t and s_r, respectively,

$$T = \frac{s_t - d_t}{t - d_t}, \tag{1}$$

$$R = \frac{s_r - d_r}{r - d_r}. \tag{2}$$

We illustrate this in Fig. 2(a) on the example of hematite, α-Fe_2O_3. These two spectra are used to approximate the spectral absorption coefficient α in the sample, which is required for Tauc plot analysis[13–16] that provides the measurement of the band gap. If reflectance is negligible, Beer-Lambert's law needs only transmittance and $\alpha \propto -ln(T)$, if not, we account for the reflectance from the front surface and $\alpha \propto -ln\frac{T}{(1-R)}$. This process is shown in Fig. 2(b). While we make every effort to achieve uniform thickness for all samples on one sample plate, the morphologies are inadvertently varied and thickness is unknown. Equally, in our geometry, we try to minimize the crosstalk between the two integrating spheres, but some light still escapes the lower sphere and registers as a part of the reflectance spectrum, which results in absorbance having values slightly lower than zero. This does not influence

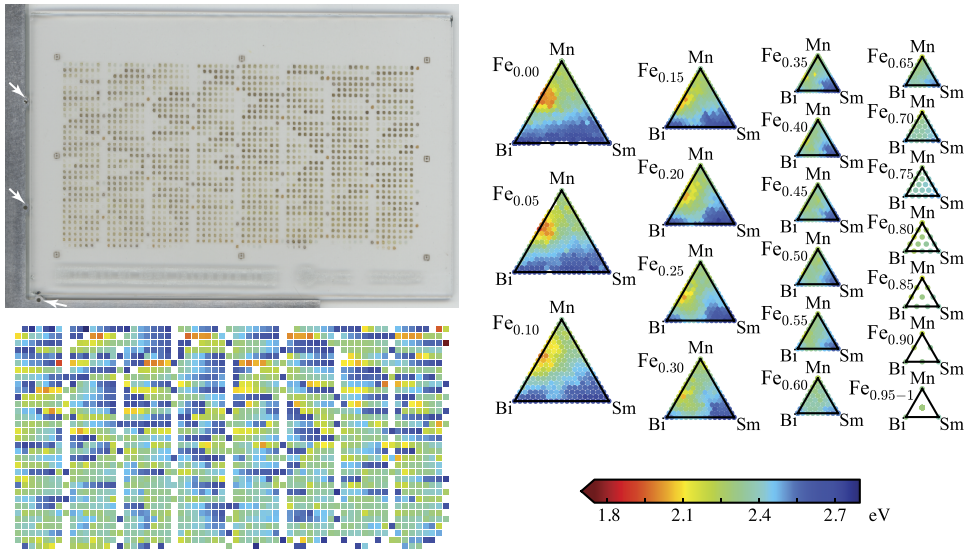

FIG. 4. (Top left) Photoscan of a combinatorial library of metal (Fe-Mn-Bi-Sm) oxides. The results of the direct bandgap extraction are mapped according to sample location in the library (bottom left) and as a series of pseudo-ternary slices with increasing Fe compositional line (right). The color scale pertains to both plots and the series of composition slices comprise the entire quaternary composition space.

the determination of band gaps, which is the primary purpose of this instrument.

Tauc plot analysis assumes that for a sufficiently high absorption coefficient, $(\alpha h\nu) \propto (h\nu - E_g)^{1/n}$, where $h\nu$ is the photon energy, and E_g is the value of the bandgap, which is direct allowed for $n = 1/2$, direct forbidden for $n = 3/2$, indirect allowed for $n = 2$, or indirect forbidden for $n = 3$. Our automated Tauc plot analysis, which we describe in detail elsewhere, measures E_g by measuring the intercept between linear segments, resulting from segmented linear fitting, corresponding to the onset of absorption, and the background region in the plot of $(\alpha h\nu)^{1/n}$ as a function of $h\nu$. This extrapolation process yields reliable results in 1.4-3.0 eV range with 0.1 eV uncertainty for the data from our instrument.

Fig. 3 illustrates the Tauc plot analysis in the case of the direct allowed bandgap for the data presented in Fig. 2. Because total absorption occurs after a certain wavelength, it is enough to take the value of the intercept of the first linear segment in the plot with the abscissa. We see again that the spectra acquired within 7 ms are adequate for measuring the direct bandgap of about 2.2 eV, a known value for hematite.

III. CASE STUDY ON COMBINATORIAL SAMPLE LIBRARY

Here, we give an example of direct bandgap extrapolation for a quaternary combinatorial library of Bi-Mn-Sm-Fe oxides prepared by inkjet printing and subsequent reactive annealing. The method of inkjet printing materials used in this example is described by Liu *et al.*[2] The materials were made by inkjet printing metal nitrate precursor solutions into an array of one square millimeter spots on glass plates with FTO. The concentration increment was 5% by number of moles of metal. The plate was annealed in air, seated on top of a silica support rack to avoid glass bowing, at 600 °C for approximately 4 h. During this process, the nitrates were combusted and the mixed metal compositions oxidized.

In Fig. 4, we show the results of the automated Tauc plot analysis which uses the reflectance and transmittance data from the Bi-Mn-Sm-Fe oxide library and as described in Subsection II C. The data are plotted according to the arrangement of samples in the library and assembled into quasi-ternary slices along the Fe compositional line. The measurement yields distinct phase regions defined by the magnitude of the direct bandgap. Note that the segmentation of the compositional space based on the bandgap is not apparent in the random spatial representation due to the unfolding of the composition space onto the array of sample locations.

We find a hot spot on the Bi-Mn compositional line with a bandgap under 2 eV, much lower than the rest of the oxides in this compositional space, and lower than the bandgap of the oxides that Bi or Mn would form under the same conditions. X-ray diffraction experiments show that this material is a known mullite phase material $Bi_2Mn_4O_{10}$.

IV. SUMMARY

Fast UV-Vis spectrometry is of particular interest for high-throughput combinatorial materials discovery. In this paper, we give the details of a scanning UV-Vis spectrometer with a dual-sphere configuration, capable of simultaneously measuring transmittance and reflectance. This is done "on-the-fly," during continuous translation of the dual-sphere scanner head. Our setup is capable of acquiring data at the overall rate better than one sample per second, limited by the stage speed in the presented configuration, with individual spectral acquisitions taking only 7 ms. The instrument can also operate in NIR, for extended spectral information.

ACKNOWLEDGMENTS

This manuscript is based upon work performed by the Joint Center for Artificial Photosynthesis, a DOE Energy Innovation Hub, supported through the Office of Science of the U.S. Department of Energy (Award No. DE-SC0004993).

[1]M. L. Green, I. Takeuchi, and J. R. Hattrick-Simpers, J. App. Phys **113**, 231101 (2013).
[2]X. Liu, Y. Shen, R. Yang, S. Zou, X. Ji, L. Shi, Y. Zhang, D. Liu, L. Xiao, X. Zheng, S. Li, J. Fan, and G. D. Stucky, Nano Lett. **12**, 5733 (2012).
[3]M. Woodhouse and B. A. Parkinson, Chem. Soc. Rev. **38**, 197 (2009).
[4]X.-D. Sun, C. Gao, J. Wang, and X.-D. Xiang, App. Phys. Lett. **70**, 3353 (1997).
[5]S. Niyomsoan, W. Grant, D. L. Olson, and B. Mishra, Thin Solid Films **415**, 187 (2002).
[6]J. Perkins, M. van Hest, C. Teplin, M. Dabney, and D. Ginley, Appl. Surf. Sci. **254**, 687 (2007).
[7]K. Stoewe, C. Dogan, F. Welsch, and W. F. Maier, Z. Phys. Chem. **223**, 561 (2013).
[8]J. B. Gerken, J. Y. C. Chen, R. C. Mass, A. B. Powell, and S. S. Stahl, Angew. Chem., Int. Ed. **51**, 6676 (2012).
[9]J. Perkins, C. Teplin, M. van Hest, J. Alleman, X. Li, M. Dabney, B. Keyes, L. Gedvilas, D. Ginley, Y. Lin, and Y. Lu, Appl. Surf. Sci. **223**, 124 (2004).
[10]M. P. Taylor, D. W. Readey, C. W. Teplin, M. F. A. M. V. Hest, J. L. Alleman, M. S. Dabney, L. M. Gedvilas, B. M. Keyes, B. To, J. D. Perkins, and D. S. Ginley, Meas. Sci. Technol. **16**, 90 (2005).
[11]S. Kirby and R. Vandover, Thin Solid Films **517**, 1958 (2009).
[12]E. Reddington, A. Sapienza, B. Gurau, R. Viswanathan, S. Sarangapani, E. S. Smotkin, and T. E. Mallouk, Science **280**, 1735 (1998), http://www.sciencemag.org/content/280/5370/1735.full.pdf.
[13]J. Tauc, *Amorphous and Liquid Semiconductors* (Plenum Press, London and New York, 1974).
[14]J. Tauc, R. Grigorovici, and A. Vancu, Phys. Status Solidi B **15**, 627 (1966).
[15]J. Tauc, Mater. Res. Bull. **3**, 37 (1968).
[16]A. Y. Anderson, Y. Bouhadana, H.-N. Barad, B. Kupfer, E. Rosh-Hodesh, H. Aviv, Y. R. Tischler, S. Ruehla, and A. Zaban, ACS Comb. Sci. **16**, 53 (2014).